This is the accepted manuscript made available via CHORUS. The article has been published as:

Direct Measurement of the Fermi Energy in Graphene Using a Double-Layer Heterostructure

Seyoung Kim, Insun Jo, D. C. Dillen, D. A. Ferrer, B. Fallahazad, Z. Yao, S. K. Banerjee, and E. Tutuc

Phys. Rev. Lett. **108**, 116404 — Published 14 March 2012

DOI: 10.1103/PhysRevLett.108.116404

Direct Measurement of the Fermi Energy in Graphene Using a Double Layer Heterostructure

Seyoung Kim,[1] Insun Jo,[2] D. C. Dillen,[1] D. A. Ferrer,[1] B. Fallahazad,[1] Z. Yao,[2] S. K. Banerjee,[1] and E. Tutuc[1]

[1]*Microelectronics Research Center, The University of Texas at Austin, Austin, TX 78758*
[2]*Department of Physics, The University of Texas at Austin, Austin, TX 78712*

(Dated: January 6, 2012)

We describe a technique which allows a direct measurement of the relative Fermi energy in an electron system by employing a double layer heterostructure. We illustrate this method by using a graphene double layer to probe the Fermi energy as a function of carrier density in monolayer graphene, at zero and in high magnetic fields. This technique allows us to determine the Fermi velocity, Landau level spacing, and Landau level broadening. We find that the $N = 0$ Landau level broadening is larger by comparison to the broadening of upper and lower Landau levels.

PACS numbers: 73.43.-f, 71.35.-y, 73.22.Gk

The Fermi energy is a fundamental property of an electron system, and thermodynamic measurements which probe the Fermi energy or density of states are key to understanding the host material band structure and electron interaction effects. Although a number of thermodynamic properties, such as specific heat [1, 2], magnetization [3], magnetocapacitance [4], or compressibility [5] can probe the density of states in an electron system, accessing them experimentally becomes increasingly difficult at the micro- and nano-scale. In the case of graphene [6], magnetization and specific heat measurements are exceedingly difficult, and the accuracy of compressibility [7] and capacitance measurements [8–10] are also limited by the reduced sample dimensions. Using a graphene double layer heterostructure, we describe a technique which allows a direct measurement of the Fermi energy in an electron system with an accuracy which is independent of the sample size. The underlying principle of the method discussed here is that an interlayer bias applied to bring the top layer to the charge neutrality point is equal to the Fermi energy of the bottom layer. We illustrate this technique by probing the Fermi energy in monolayer graphene, both at zero and in high magnetic fields. We show that this method allows an accurate determination of the Fermi velocity, Landau level spacing, and Landau level broadening in monolayer graphene.

Our samples are independently contacted graphene double layers, consisting of two graphene single layers separated by a thin dielectric as shown in Fig. 1(a) [11]. To fabricate such devices, we first mechanically exfoliate the bottom graphene layer from natural graphite onto a 280 nm thick SiO_2 dielectric, thermally grown on a highly doped Si substrate. Standard e-beam lithography, Cr/Au deposition followed by lift-off, and O_2 plasma etching are used to define a Hall bar device. A 4 to 7 nm top Al_2O_3 dielectric layer is deposited on the bottom layer by atomic layer deposition (ALD), and using evaporated Al as a nucleation layer. The dielectric film thickness grown on graphene is further verified by transmission electron microscopy in multiple samples. To fabricate the graphene top layer, a separate graphene single layer is mechanically exfoliated on a SiO_2/Si substrate. After spin-coating polymetyl metacrylate (PMMA) on the top layer and curing, we etch the underlying substrate with NaOH, and detach the top layer along with the alignment markers captured in the PMMA membrane. The membrane is transferred onto the bottom layer device, and aligned. A Hall bar is subsequently defined on the top layer, completing the double layer graphene device. Three samples were investigated in this study, all with similar results. We focus here on data collected from one sample with a 7.5 nm thick interlayer dielectric, and with an interlayer resistance larger than 1 GΩ. Both layer mobilities are 10,000 cm^2/V·s. Using small signal, low frequency lock-in techniques we probe the layer resistivities as a function of back-gate bias (V_{BG}), and the inter-layer bias (V_{TL}) applied on the top layer. The bottom layer is maintained grounded during measurements.

Figure 1(b,c) data show the longitudinal resistivity of the bottom (ρ_B) and top (ρ_T) layer measured as a function of V_{TL}, and at different V_{BG} values [12]. The data $\rho_{B,T}$ vs. V_{TL} exhibit the ambipolar behavior characteristic of graphene, and with a charge neutrality point which is V_{BG}-dependent. The shift of the charge neutrality point of the bottom layer as a function of V_{BG} is explained by picturing the bottom layer as a dual-gated graphene single layer, with the Si substrate as back-gate and the top graphene layer serving as top-gate. The dependence of the ρ_T vs. V_{TL} data on V_{BG} is more subtle, and implies an incomplete screening by the bottom layer of the back-gate induced electric field.

We can quantitatively explain the top (n_T) and bottom (n_B) layer carrier density dependence on V_{BG} and V_{TL} using a band diagram model [Figs. 1(d,e)]. An applied V_{BG} is the sum of the potential drop across the SiO_2 dielectric and the Fermi energy of the bottom layer:

$$eV_{BG} = e^2(n_B + n_T)/C_{SiO_2} + E_F(n_B) \qquad (1)$$

Here, $E_F(n)$ represents the Fermi energy measured from the charge neutrality point at a carrier density n; $n_{B,T}$

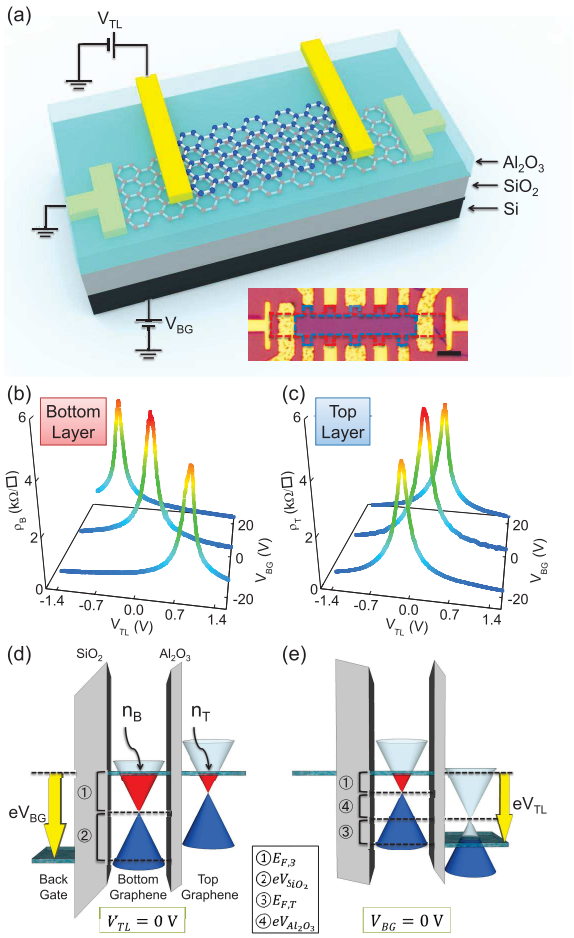

FIG. 1: (color online) (a) Schematic representation of a graphene double layer separated by an Al_2O_3 dielectric, and with a bottom SiO_2 dielectric. A back-gate (V_{BG}) and inter-layer (V_{TL}) bias can be applied on the Si substrate and top layer, respectively. Lower right: optical micrograph of a graphene double layer device. The red (blue) contour marks the bottom (top) layer. The scale bar is 5 μm. (b,c) Layer resistivities measured as a function of V_{TL} and V_{BG} at $T = 0.4$ K. (d,e) Band diagram of a graphene double layer under an applied back-gate [panel (d)] or inter-layer [panel (e)] bias.

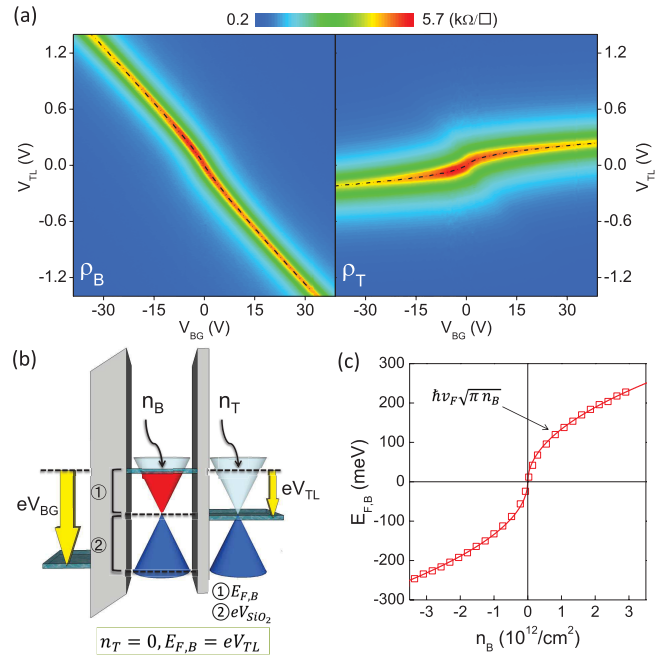

FIG. 2: (color online) (a) Contour plots of ρ_B (left) and ρ_T (right) measured as a function of V_{BG} and V_{TL}, at $T = 0.4$ K. (b) Band diagram of a graphene double layer with the top layer at the charge neutrality point. The inter-layer bias is equal to the bottom layer Fermi energy. (c) Bottom layer Fermi energy vs. carrier concentration, determined using data of panel (a). The symbols are experimental data, while the solid line represents the expected $\hbar v_F\sqrt{\pi n_B}$ dependence.

and $E_F(n)$ are positive when the carriers are electrons, and negative when the carriers are holes. C_{SiO_2} denotes the bottom dielectric capacitance per unit area. Similarly to Eq. (1), the applied V_{TL} bias can be written as the sum of the potential drop across the Al_2O_3 dielectric and the Fermi energies of the two layers:

$$eV_{TL} = E_F(n_B) - (E_F(n_T) + e^2 n_T/C_{Al_2O_3}) \quad (2)$$

$C_{Al_2O_3}$ is the inter-layer dielectric capacitance per unit area. Figure 1 shows two examples of band diagrams in the graphene double layer, at finite V_{BG} and $V_{TL} = 0$ V [Fig. 1(d)], as well as finite V_{TL} and $V_{BG} = 0$ V [Fig. 1(e)]. For simplicity the back-gate Fermi energy and the two graphene layers charge neutrality points are assumed to be aligned at $V_{BG} = 0$ V and with both layers at ground potential. In Fig. 1(e) the V_{TL} bias is assumed to be positive, resulting in electrons (holes) induced in the bottom (top) layer. We emphasize that no assumptions are made with regard to the E_F dependence on n_B and n_T. As we show below, this dependence will be determined experimentally.

Figure 2(a) data show contour graphs of ρ_B (left panel) and ρ_T (right panel) as a function of V_{BG} and V_{TL}. The bottom layer resistivity dependence on gate and inter-layer bias is very similar to a dual-gated graphene monolayer, showing an almost linear dependence of the charge neutrality point on V_{BG} and V_{TL}, with a slope equal to the $C_{SiO_2}/C_{Al_2O_3}$ ratio. Using $C_{SiO_2} = 12$ nF/cm^2 for the bottom SiO_2 dielectric, we determine the inter-layer dielectric capacitance to be $C_{Al_2O_3} = 340$ nF/cm^2 [13]. The capacitance values are confirmed by Hall measurements.

The top layer resistivity shows the characteristic ambipolar behavior as a function of V_{TL}, but with a weaker V_{BG} dependence. Let us examine more closely the top layer charge neutrality point dependence on V_{BG} and V_{TL}. If we consider the top layer at the charge neutrality point, setting $n_T = 0$ in Eq. (2) yields:

$$eV_{TL} = E_F(n_B) \quad (3)$$

This equation contains a simple, yet remarkable result.

The inter-layer bias required to bring the top layer at the charge neutrality point is equal to the Fermi energy of the opposite layer, in units of eV [Fig. 2(b)]. Consequently, tracking the top layer charge neutrality point in the V_{BG} - V_{TL} plane [dash-dotted trace in Fig. 2(a) left panel], results in a measurement of the bottom layer Fermi energy as a function of V_{BG}. Furthermore, setting $n_T = 0$ in Eq. (1), and using Eq. (3) allows for n_B to be determined as a function of V_{BG} and V_{TL} along the top layer charge neutrality line of Fig. 2(a):

$$V_{BG} - V_{TL} = en_B/C_{SiO_2} \tag{4}$$

Equations (3) and (4) provide a direct measurement of the bottom layer Fermi energy as a function of density. To illustrate this, in Fig. 2(c) we show the bottom layer Fermi energy $E_{F,B}$ as a function of n_B, determined using Fig. 2(a) data and Eqs. (3) and (4). The E_F values are in excellent agreement with the $E_F(n_B) = \hbar v_F\sqrt{\pi n_B}$ dependence expected for the linear energy-momentum dispersion of graphene, and with an extracted Fermi velocity of $v_F = 1.15 \times 10^8$ cm/s.

In the following we show that the above method applies equally well to an electron system in high magnetic fields, allowing a direct measurement of Landau level (LL) energies and broadening. In Fig. 3(a) we show the contour plots of ρ_T (top panel) and ρ_B (bottom panel) measured as a function of V_{BG} and V_{TL} in an applied perpendicular magnetic field $B = 8$ T. Both layers show quantum Hall states (QHS) marked by vanishing resistivities at filling factors $\nu = 4(N + \frac{1}{2})$, consistent with monolayer graphene [14, 15]. The integer N represents the Landau level index. The top panel of Fig. 3(a) data shows a step-like dependence of the top layer charge neutrality point on V_{BG} and V_{TL}. Similarly to Fig. 2, substituting eV_{TL} with $E_{F,B}$ at the top layer charge neutrality line in Fig. 3(a) (top panel) provides a mapping of $E_{F,B}$ as a function of V_{BG}. To visualize this, the top layer charge neutrality line in the $V_{BG} - V_{TL}$ plane is superposed with the ρ_B contour plot of Fig. 3(b) (bottom panel), which shows step-like increments of $E_{F,B}$ coinciding with the bottom layer QHSs.

Figure 3(b) shows $E_{F,B}$ vs. n_B at $B = 8$ T determined by tracking the top layer charge neutrality line in the $V_{TL} - V_{BG}$ plane in Fig. 3(a), and using Eqs. (3) and (4) to convert V_{TL} and V_{BG} into $E_{F,B}$ and n_B, respectively. In addition, Fig. 3(b) shows ρ_B vs. $E_{F,B}$, determined by tracking the bottom layer resistivity along the top layer charge neutrality line [dashed-dotted line of Fig. 3(a)]. Figure 3(b) data manifestly shows the staircase-like behavior expected for the Fermi level dependence on density for a two-dimensional electron system in a perpendicular magnetic field. The peaks in the ρ_B vs. $E_{F,B}$ data of Fig. 3(b), corresponding to the Fermi level lying in the LL center and probing extended states, correlate with plateaus in the $E_{F,B}$ vs. n_B, associated with the large LL density of states. The peaks in the ρ_B vs. $E_{F,B}$

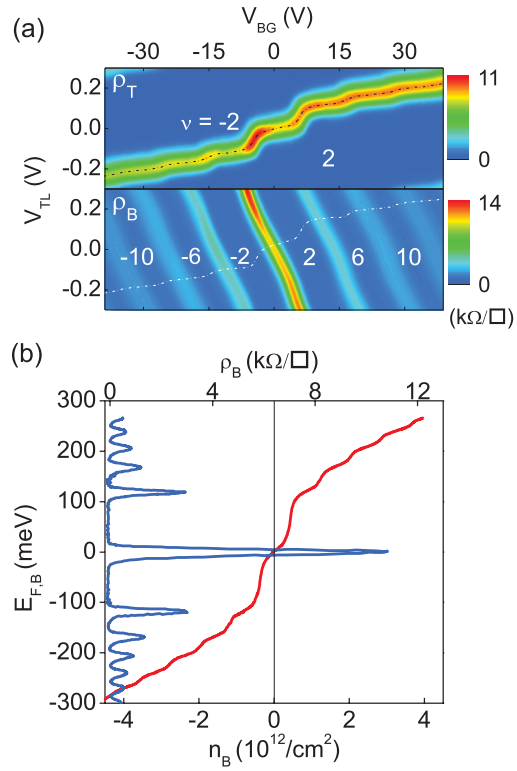

FIG. 3: (color online) (a) ρ_T (top) and ρ_B (bottom) contour plots measured as a function of V_{BG} and V_{TL} at $B = 8$ T, and $T = 0.4$ K. Both layers show quantum Hall states marked by vanishing longitudinal resistance at filling factors $\nu = \pm 2, 6, 10$, consistent with mono-layer graphene. The top layer charge neutrality line (dashed line) shows a step-like behavior, with the steps matching the bottom layer quantum Hall states. (b) ρ_B (blue line, top axis) vs. $E_{F,B} = eV_{TL}$, and $E_{F,B}$ vs. n_B (red line, bottom axis) determined from the top layer charge neutrality line of panel (a). The $E_{F,B}$ values at the peak positions of ρ_B provide the Landau level energies.

data of Fig. 3(b) provide a direct measurement of the LL energy. Figure 4(a) summarizes the bottom graphene layer LL energy as a function of index (N) at $B = 8$ T. The experimental data is in excellent agreement with the theoretical dependence $E_N = \pm v_F\sqrt{2\hbar eB|N|}$, corresponding to a Fermi velocity $v_F = 1.17 \times 10^8$ cm/s, a value less than 2% different than the Fermi velocity determined at $B = 0$ T using Fig. 2 data.

In Figure 4(b) we compare the $E_{F,B}$ vs. n_B data determined experimentally at $B = 8$ T, with calculations. Assuming a Lorentzian distribution of the disorder-induced LL broadening, the density of states $D(E)$ writes:

$$D(E) = \frac{4e}{h}B\sum_N \frac{1}{\pi}\frac{\gamma_N}{(E - E_N)^2 + \gamma_N^2} \tag{5}$$

with γ_N being the broadening of the N-th LL. The carrier density (n) dependence on E_F in the limit $T = 0$ K is:

$$n(E_F) = \int_0^{E_F} D(E)dE \tag{6}$$

Using Eqs. (5) and (6), the best fit to $E_{F,B}$ vs. n_B data is obtained for $\gamma_0 = 14$ meV, and $\gamma_N = 6.5$ meV for $|N| > 0$. The summation in Eq. (5) does not converge if carried out to infinity, and a high-energy cut-off is customarily used. For the calculations of Fig. 4(b) we used $|N| \leq 100$ in Eq. (5), corresponding to a 1 eV cut-off energy; increasing the cut-off LL index to 1,000, will change the best fit γ value by less than 0.5 meV. The lower inset of Fig. 4(b) shows a comparison of the $E_{F,B}$ vs. n_B experimental data with calculations using the same broadening for the $N = 0$ LL as the upper and lower LLs, $\gamma = 6.5$ meV. The larger broadening of the $N = 0$ LL by comparison to the other LLs is an interesting finding. A theoretical study [16], which examined the impact of static disorder on LL broadening in graphene without considering interaction showed that the $N = 0$ LL broadening is the same as for the other LLs. On the other hand electron-electron interaction can impact the broadening of the four-fold degenerate $N = 0$ LL, and experimental data on exfoliated graphene on SiO_2 substrates show a splitting of the $N = 0$ LL in high, $B = 45$ T magnetic fields [17], explained as a many-body effect. Lastly, we note that a Gaussian-shaped Landau levels density of states yields worse fits to Fig. 4 data, by comparison to the Lorentzian shape density of states. Scanning tunneling microscopy [18, 19], and compressibility studies in graphene [7] also favor the Lorentzian LL line-shape by comparison to the Gaussian one. A recent theoretical study argues that LL local density of states has a Lorentzian lineshape while the total density of states is Gaussian [20]. Presumably, the sample size examined here, defined by a 4 μm Hall bar width coupled with the 8 μm top layer contact spacing is sufficiently small such that the Lorentzian LL line-shape dominates.

In summary, we present a method to determine the Fermi energy in a two-dimensional electron system, using a graphene double layer heterostructure. We illustrate this technique by probing the Fermi energy in graphene monolayer at zero and in a high magnetic field, and determine with high accuracy the Fermi velocity, Landau level spacing and broadening.

We thank C. P. Morath and M. P. Lilly for technical discussions. This work was supported by NRI, ONR, and Intel. Part of this work was performed at the National High Magnetic Field Laboratory, which is supported by NSF (DMR-0654118), the State of Florida, and the DOE.

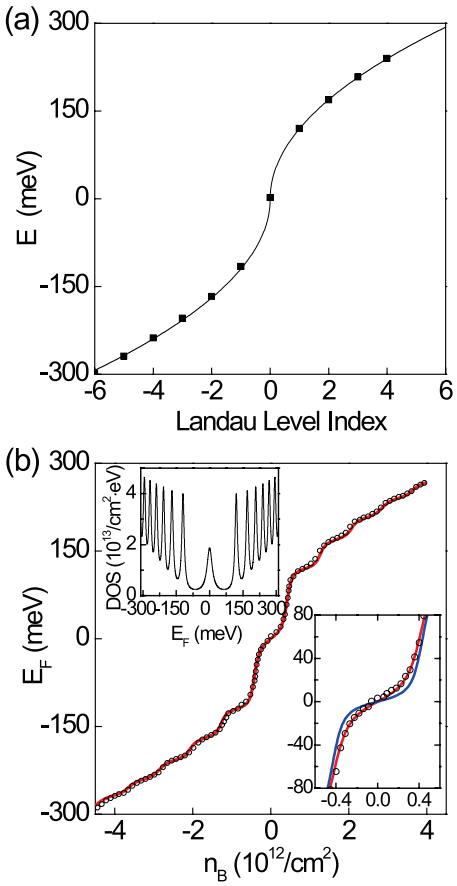

FIG. 4: (color online) (a) Landau level energy in monolayer graphene as a function of index (N). The symbols are experimental data determined from the $E_{F,B}$ positions at the ρ_B peaks in Fig. 3(b). The solid line is the theoretical $\pm v_F\sqrt{2\hbar eB|N|}$ dependence using $v_F = 1.17 \times 10^8$ cm/s. (b) $E_{F,B}$ vs. n_B at $B = 8$ T. The symbols represent experimental data, and the solid (red) line is a fit assuming a Landau level Lorentzian line shape. The best fit is obtained for $\gamma_N = 6.5$ meV for $|N| > 0$, and $\gamma_0 = 14$ meV. The upper inset shows the calculated density of states corresponding to the best fit to experimental data. The lower inset shows the E_F vs. n_B data in the vicinity of zero density. The symbols represent experimental data, and the lines are calculations assuming $\gamma_0 = 6.5$ meV (blue line) and $\gamma_0 = 14$ meV (red line).

[1] E. Gornik *et al.*, Phys. Rev. Lett. **54**, 1820 (1985).
[2] J. K. Wang *et al.*, Phys. Rev. B **45**, 4384 (1992).
[3] J. P. Eisenstein *et al.*, Phys. Rev. Lett. **55**, 875 (1985).
[4] T. P. Smith *et al.*, Phys. Rev. B **32**, 2696 (1985).
[5] J. P. Eisenstein, L. N. Pfeiffer, and K. W. West, Phys. Rev. B **50**, 1760 (1994).
[6] A. K. Geim, K. S. Novoselov, Nature Materials **6**, 183 (2007).
[7] E. A. Henriksen, and J. P. Eisenstein, Phys. Rev. B **82**, 041412(R) (2010).
[8] L. A. Ponomarenko *et al.*, Phys. Rev. Lett. **105**, 136801 (2010).
[9] A. F. Young *et al.*, arXiv:1004.5556 (2010).
[10] S. Droscher *et al.*, Appl. Phys. Lett. **96**, 152104 (2010).
[11] S. Kim *et al.*, Phys. Rev. B **83**, 161401 (2011).
[12] For simplicity V_{BG} and V_{TL} are referenced with respect the bias values at which both layers are at the Dirac point: $V_{BG} = 8$ V, $V_{TL} = -0.01$ V.
[13] The ALD Al_2O_3 used here has a dielectric constant of 6, and the graphene/Al_2O_3 interfaces add series contributions to the inter-layer capacitance; B. Fallahazad *et al.*, 69th Dev. Res. Conf. Digest, 35 (2011).
[14] K. S. Novoselov *et al.*, Nature **438**, 197 (2005).
[15] Y. Zhang *et al.*, Nature **438**, 201 (2005).
[16] W. Zhu *et al.*, Phys. Rev. Lett. **102**, 056803 (2009).
[17] Y. Zhang *et al.*, Phys. Rev. Lett. **96**, 136806 (2006).
[18] G. Li, A. Luican, E. Y. Andrei, Phys. Rev. Lett. **102**, 176804 (2009).
[19] D. L. Miller *et al.*, Science **324**, 924 (2009).
[20] W. Zhu *et al.*, Phys. Rev. B **83**, 153408 (2011).